KeAi
CHINESE ROOTS
GLOBAL IMPACT

Contents lists available at ScienceDirect

Journal of Holistic Integrative Pharmacy

journal homepage: www.keaipublishing.com/en/journals/journal-of-holistic-integrative-pharmacy



Integrating metabolism gene clusters and tumor immune microenvironment in head and neck squamous cell carcinoma



Meina Lian^{a,1}, Xiaoxia Wang^{a,1}, Zixian Huang^b, Yudong Wang^{a,*}, Zhiquan Huang^{a,b,**}

- a First Affiliated Hospital of Guangdong Pharmaceutical University, Guangzhou, 510062, China
- b Department of Oral and Maxillofacial Surgery, Sun Yat-sen Memorial Hospital, Sun Yat-sen University, Guangzhou, 510120, China

ARTICLE INFO

Keywords:
Head and neck squamous cell carcinoma
(HNSCC)
TNFAIP6
Metabolism
Tumor immune microenvironment

ABSTRACT

Objective: To investigate the relationship between tumor metabolism and immune cell infiltration in Head and Neck Squamous Cell Carcinoma (HNSCC), aiming to identify novel biomarkers and potential therapeutic targets. *Methods:* Seven major metabolic pathways were analyzed using Gene Set Variation Analysis (GSVA) in HNSCC cohorts to assess their correlation with overall survival (OS) and immune microenvironment characteristics. Unsupervised clustering was applied to identify metabolic subtypes, and differentially expressed metabolism-related genes (MRGs) were screened for prognostic relevance. A risk model was constructed based on 16 core MRGs. TNFAIP6 was further evaluated for its functional role through *in vitro* assays, including proliferation, migration, and invasion analyses.

Results: The activity of key metabolic pathways, such as glycolysis, oxidative phosphorylation, and fatty acid metabolism, significantly correlated with OS and immune infiltration patterns. Two distinct metabolic clusters (C1 and C2) were identified, with C1 associated with a more immune-enriched microenvironment. A total of 698 MRGs were linked to immune modulation and tumor progression. The risk model based on 16 MRGs effectively stratified patients by prognosis and immune infiltration status. TNFAIP6 was highly expressed in malignant cells and associated with immunosuppression, poor survival, and tumor progression. Functional experiments confirmed that TNFAIP6 knockdown inhibited tumor cell proliferation, migration, and invasion.

Conclusion: Metabolic reprogramming plays a critical role in shaping the immune landscape of HNSCC. TNFAIP6 represents a promising prognostic biomarker and potential therapeutic target for improving personalized treatment in HNSCC patients.

1. Introduction

Head and Neck Squamous Cell Carcinoma (HNSCC) is one of the most prevalent malignant cancers in the world, with its development strongly linked to risk factors like smoking, alcohol use, and HPV infection. Although advances in early diagnosis and treatment have been made, the high recurrence rate and low survival rate continue to pose major obstacles in clinical management.

In recent years, tumor metabolism research has gradually become an important field of tumor immunology.³ Tumor cells are key players in metabolic reprogramming, which not only promotes their proliferation, survival, and migration, but also influences immune responses in the

tumor microenvironment.⁴ Within the tumor immune microenvironment (TIME), the functionality and infiltration patterns of immune cells exert a profound influence on tumor immune evasion, therapeutic responsiveness, and patient prognosis.⁵

Metabolic pathways are pivotal in modulating immune cell activity and shaping the TIME, with specific pathways such as glycolysis, oxidative phosphorylation, fatty acid metabolism, and amino acid metabolism being closely intertwined with the immunosuppressive tumor microenvironment. Consequently, delving into the impact of these metabolic pathways on the immune microenvironment could yield novel biomarkers and therapeutic targets for the management of HNSCC. However, few studies have conducted genomic analyses of

Peer review under the responsibility of Editorial Board of Journal of Holistic Integrative Pharmacy.

^{*} Corresponding author. First Affiliated Hospital of Guangdong Pharmaceutical University, Guangzhou, 510062, China.

^{**} Corresponding author. First Affiliated Hospital of Guangdong Pharmaceutical University, Guangzhou, 510062, China. *E-mail addresses*: dong3295@139.com (Y. Wang), hzhquan@mail.sysu.edu.cn (Z. Huang).

¹ Joint first author: these authors contributed to this work equally.

HNSCC from a global perspective of metabolic heterogeneity. Most previous research has been limited to specific metabolic pathways.^{7,8}

This study aims to deeply explore the interaction between the seven metabolic pathways, rather than focusing solely on individual pathways and the immune microenvironment in HNSCC based on bioinformatics analysis. Through systematic analysis of tumor-related genes, we hope to reveal the relationship between specific metabolic pathways and immune cell infiltration, thereby providing new insights and directions for tumor immunotherapy.

2. Methods and materials

2.1. Data acquisition

RNA sequencing (RNA-seq) data and corresponding clinical information for 519 HNSCC samples were retrieved from The Cancer Genome Atlas (TCGA) database (https://portal.gdc.cancer.gov/). For external validation, the GSE65858 dataset, comprising 270 HNSCC patients with gene expression profiles and clinical data, was downloaded from the Gene Expression Omnibus (GEO) database (https://www.ncbi.nlm.nih.gov/geo/). All TCGA data were accessed and downloaded prior to the implementation of access restrictions, ensuring that the analyses conducted in this study are not impacted by current database limitations. All GEO data used in this study are publicly available and were accessed in accordance with data usage policies.

The gene sets representing seven major metabolic pathways were previously identified by Peng et al. These pathways encompass amino acid metabolism, carbohydrate metabolism, energy metabolism integration, lipid metabolism, nucleotide metabolism, the tricarboxylic acid (TCA) cycle, and vitamin & cofactor metabolism (Supplementary Table S1).

2.2. Pathway enrichment analysis

Gene set variation analysis (GSVA) was conducted using the "GSVA" R package to assess the activity of seven metabolic pathways in each tumor sample. This method calculates enrichment scores for each pathway based on the expression levels of relevant gene sets. The enrichment scores for all samples are listed in Supplementary Table S2.

Kaplan-Meier survival analysis and log-rank tests were used to evaluate the connection between the activity of these metabolic pathways and overall survival (OS) in HNSCC patients. The analysis was conducted using Sangerbox 3.0 (http://sangerbox.com/home.html). To determine the optimal cut-off point for categorizing pathway activity levels, the "surv_cutpoint" function from the "survminer" R package was utilized. This function identifies the cut-off value that maximizes the logrank statistic, ensuring an optimal separation of patients into high- and low-activity groups for each pathway.

2.3. Identification of metabolic pathway-related clusters

After identifying key metabolic pathways associated with prognosis in HNSCC, clustering analysis was conducted using the ConsensusClusterPlus tool¹⁰ to identify potential metabolic subtypes. The analysis used PAM clustering with Pearson correlation distance (1-Pearson correlation) and performed 10-fold resampling with 80% of the samples in each iteration.

The optimal number of clusters (K) was determined using the empirical cumulative distribution function (CDF) plot. As the number of clusters (K) increases, the area under the CDF curve also increases. To select the optimal K, we considered the following two factors: (1) the area under the CDF curve, which should be maximized, and (2) the trend in the CDF Delta plot, where the optimal K is selected when the Delta decrease is slowest. After evaluating these factors, the final decision was made. Additionally, consistency within clusters was considered, where the cluster with the highest average within-cluster consistency was

chosen as K=2, and the second highest as K=3. Based on these analyses, HNSCC samples were classified into two distinct metabolic clusters.

2.4. Immune infiltration analysis

The ESTIMATE algorithm was used to assess the overall level of immune infiltration in tumor tissues based on gene expression data, a widely used method in previous studies. 11,12 This algorithm provided three key scores: ImmuneScore, StromalScore, and ESTIMATEScore (the latter being inversely correlated with tumor purity), which were calculated for patients with HNSCC. In addition, immune cell infiltration scores for 22 immune cell types were calculated using the CIBERSORT tool (R package IOBR), providing a more detailed analysis of the immune microenvironment in each sample. 13

2.5. Identification of metabolism-related genes (MRGs) in HNSCC

Differentially expressed genes (DEGs) between different metabolic pathway-related clusters were identified using the "limma" package in R, with a threshold of P < 0.05 and log2|fold change| ≥ 1.00 . Genes meeting these criteria were considered as MRGs.

Subsequently, Kyoto Encyclopedia of Genes and Genomes (KEGG) pathway analysis was conducted to explore the biological functions and pathways associated with MRGs. The prognostic significance of MRGs in HNSCC was evaluated using univariate Cox regression. After identifying prognosis-related MRGs, potential gene clusters associated with MRGs were determined through unsupervised clustering analysis.

2.6. Risk model construction

In this study, we narrowed down the MRGs associated with HNSCC and identified key prognostic genes using univariate Cox regression and Lasso regression analysis. The selected key prognostic genes were then included in a stepwise multivariate regression model to construct the risk model. The model with the highest C-index was chosen as the optimal risk model. To evaluate the predictive accuracy of the risk score, time-dependent ROC curves were generated using the time ROC R package, which is commonly used to estimate ROC curves and the area under the curve (AUC) when dealing with censored data. ¹⁴ The inverse probability weighting method was used to manage censored data during the estimation process.

2.7. Cell culture and transfection

The human oral adenosquamous carcinoma cell line Cal-27 and the human oral squamous cell carcinoma cell line HSC-6 were obtained from the American Type Culture Collection (ATCC, USA). Cells were cultured in Dulbecco's Modified Eagle Medium (DMEM) supplemented with 10% fetal bovine serum (FBS) and 1% penicillin–streptomycin, and maintained at $37~^{\circ}$ C in a humidified incubator with 5% CO₂.

Transient transfections were performed using Lipofectamine 2000 (Invitrogen, Carlsbad, USA) according to the manufacturer's protocol. Small interfering RNAs (siRNAs) targeting TNFAIP6 were synthesized by GenePharma (Suzhou, China) and transfected using the same reagent. The sequences of the siRNAs are provided in Supplementary Table S11.

2.8. Cell proliferation assay

Transfected cells were cultured for 24 h, then seeded at a density of 2000 cells per well in a 96-well plate. After cell adhesion, they were incubated for 1, 3, and 5 days. At each time point, 10 μL of MTT reagent was added to each well, and cells were incubated for 4 h at 37 $^{\circ} C$. The reaction was stopped by adding 100 μL of 10% sodium dodecyl sulfate (SDS) solution, and absorbance was measured at 570 nm using a microplate reader. The experiment was repeated three times to ensure

result accuracy and reproducibility.

2.9. Colony formation assay

CAL-27 and HSC-6 cells with TNFAIP6 knockdown were seeded at 500 cells per well in 12-well plates and cultured for 14 days to allow colony formation. After incubation, the colonies were fixed with 4% paraformaldehyde at room temperature for 30 min, then stained with 0.1% crystal violet for 30 min. Excess dye was removed by washing the stained colonies with PBS, air-dried, and then counted manually under a microscope.

2.10. Cell invasion and migration assay

Cell invasion and migration abilities were assessed using the Transwell system and scratch assay respectively. For the invasion assay, cells were resuspended in serum-free medium and placed into the upper chamber of a Transwell system (8 μm pore size, Corning). The lower chamber contained medium with 20% fetal bovine serum (FBS) as a chemoattractant. After 24 h of incubation, non-invasive cells on the upper surface of the membrane were removed using a cotton swab. The invaded cells on the lower surface were then fixed, stained with crystal violet, and counted under a microscope.

For the scratch assay, transfected cells were seeded into 12-well

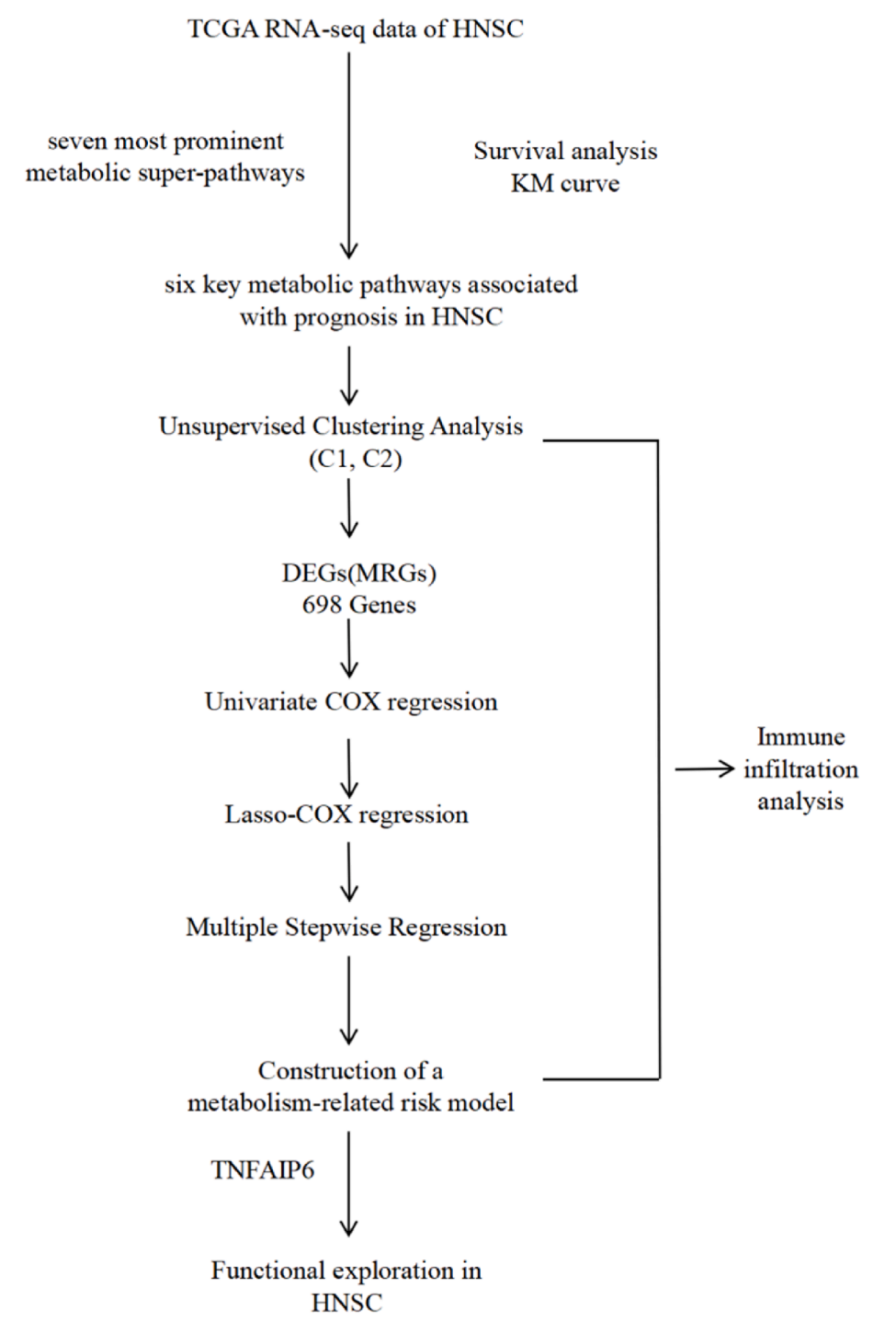


Fig. 1. Flowchart of the development of the risk model and identification of key factors in HNSCC.

plates and allowed to adhere. Once adhered, a scratch was made across the cell monolayer using a sterile pipette tip, and the cells were incubated for 24 h in serum-free medium. Migration was observed and quantified by imaging the wound area at 0 and 24 h.

2.11. RNA extraction and RT-qPCR

Total RNA was isolated from cultured cells using TRIzol reagent (Invitrogen, #15596018) (1 mL per well), following the manufacturer's instructions. The extraction process involved the addition of chloroform, isopropanol, and 75% ethanol for RNA purification. After extracting

RNA, its concentration was measured using a NanoDrop spectrophotometer. For cDNA synthesis, 1 μg of total RNA was reverse-transcribed using a reverse transcription kit (Takara, #RR047A) according to the manufacturer's instructions. Quantitative PCR (RT-qPCR) was then performed with specific primers listed in Supplementary Table S11. The RT-qPCR was carried out in a 10 μL reaction volume, and gene expression was normalized to the housekeeping gene actin.

2.12. Statistical analysis

Differences between two groups were analyzed using either an

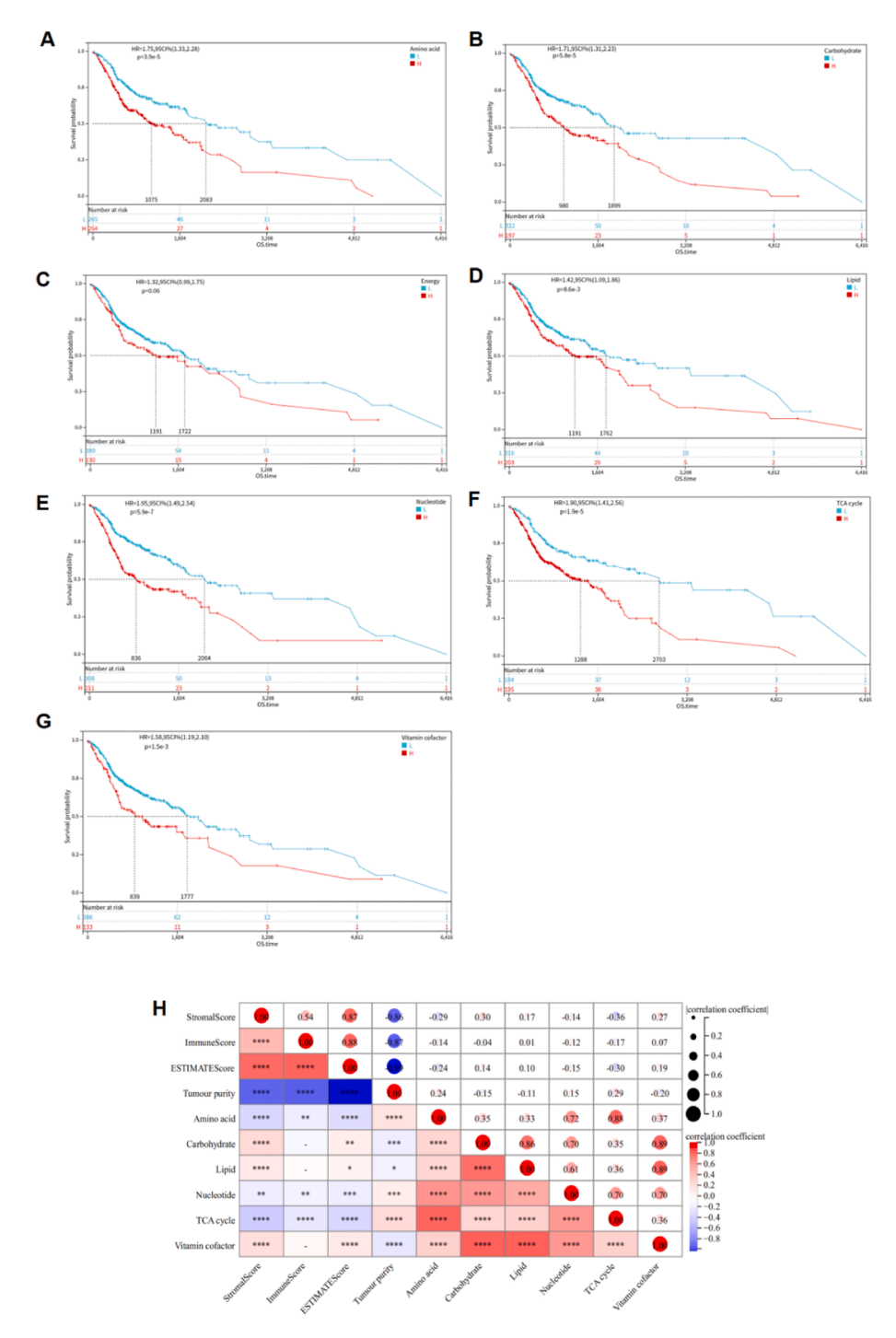


Fig. 2. Prognostic relevance of metabolic pathway activity and its association with the tumor microenvironment in HNSCC. A—G. KM survival curves for overall survival (OS) based on the activity of seven metabolic pathways. H. Correlation heatmap showing the association of metabolic pathway activity with immune infiltration scores and tumor purity.

unpaired Student's t-test or the Wilcoxon rank sum test, based on the data distribution. For comparisons involving more than two groups, one-way ANOVA or the Kruskal-Wallis test was applied, as appropriate. Spearman's correlation analysis was used to assess the relationship between two variables. A two-sided P-value of <0.05 was considered statistically significant, unless stated otherwise. All statistical analyses were conducted using R software (Version 4.4.2).

3. Results

3.1. Identification of key metabolic pathways in HNSCC

The flowchart was shown in Fig. 1. To explore the role of metabolic pathways in HNSCC, we conducted Gene Set Variation Analysis (GSVA) on RNA-seq data to measure the activity of seven key metabolic

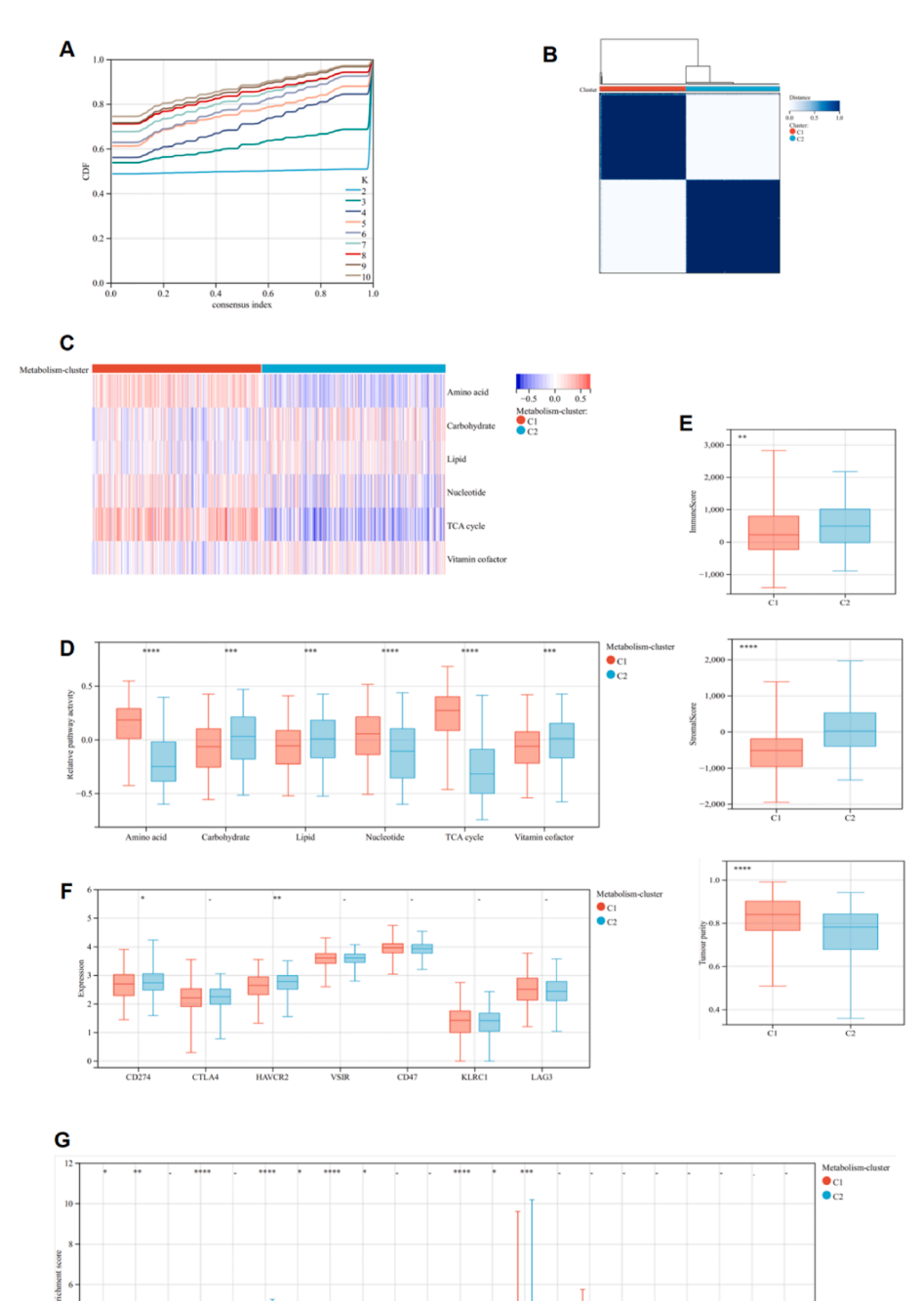


Fig. 3. Identification of metabolic pathway-related clusters and their association with TIME in HNSCC. A. Cumulative distribution function (CDF) curve for consensus clustering. B. Heatmap of consensus clustering, categorizing HNSCC samples into two metabolism-related clusters (C1 and C2). C. Heatmap depicting the activity of six metabolic pathways across the two clusters. D. Boxplots displaying the GSVA scores of the six key metabolic pathways between clusters. E. Boxplots comparing immune infiltration scores and tumor purity between the two clusters. F. Boxplots comparing the expression levels of immune checkpoints between C1 and C2. G. Boxplots illustrating differences in the infiltration of various immune cell types between the two clusters. *P < 0.05, **P < 0.01, ***P < 0.001, ****P < 0.0001,compared to Cluster C1.

pathways in tumor samples (Supplementary Table S2). Using the GSVA scores, samples were divided into high-activity and low-activity groups for each pathway, based on optimal cut-off values determined through survival analysis.

Kaplan-Meier survival curves showed a significant correlation between the metabolic activity of the seven pathways and overall survival (OS) in HNSCC patients (Fig. 2A–G). Specifically, pathways such as amino acid metabolism, carbohydrate metabolism, lipid metabolism, nucleotide metabolism, the tricarboxylic acid (TCA) cycle, and vitamin and cofactor metabolism showed that patients with higher pathway activity exhibited significantly improved OS compared to those with lower activity (log-rank test, P < 0.05).

Interestingly, energy metabolism was the only pathway where GSVA scores failed to demonstrate a significant correlation with OS, suggesting that its activity may not be a critical determinant of survival outcomes in HNSCC. These findings highlight the heterogeneity in the prognostic relevance of metabolic pathways and underscore the potential importance of specific metabolic activities in influencing tumor progression and patient outcomes.

The relationship between these six key metabolic pathways and the overall level of immune infiltration in HNSCC was initially examined.

Further analysis uncovered distinct relationships between the activity of these metabolic pathways and the tumor microenvironment. A robust positive correlation prevails among the immune infiltration levels (Supplementary Table S3). Specifically, among the six pathways significantly associated with overall survival, only amino acid metabolism, nucleotide metabolism, and the TCA cycle exhibited a negative correlation with immune infiltration levels (Fig. 2H). Conversely, the activity of these three pathways was positively correlated with tumor purity, suggesting a potential role in shaping an immunosuppressive tumor microenvironment. These findings imply that heightened activity in these pathways may contribute to reduced immune cell infiltration, while promoting a tumor-dominated microenvironment.

3.2. Identification of metabolic pathway-related clusters and their association with TIME in HNSCC

To further investigate the relationship between metabolic activity and TIME in HNSCC, unsupervised consensus clustering was performed based on the GSVA scores of six key metabolic pathways significantly associated with OS. The optimal number of clusters was determined to be two (k=2) using the cumulative distribution function (CDF) and consensus matrix stability analysis (Fig. 3A and B).

These two clusters, designated as C1 and C2 (Supplementary Table S4), exhibited distinct metabolic activity profiles (Fig. 3C). Cluster C1 was characterized by significantly higher activity of amino acid metabolism, nucleotide metabolism, and the TCA cycle compared to Cluster C2, while Cluster C2 exhibited higher activity in carbohydrate, lipid, and vitamin & cofactor metabolism (Fig. 3D).

We also investigated the connection between metabolic clusters and the TIME in HNSCC. Cluster C2 displayed features indicative of a more immune-enriched TIME, including higher ImmuneScore and Stromal-Score, alongside lower tumor purity (Fig. 3E), suggesting higher immunosuppression in C1.

Furthermore, Cluster C2 demonstrated elevated expression of key immune checkpoint molecules such as CD274 (PD-L1) and HAVCR2, suggesting a more immune-active phenotype compared to Cluster C1 (Fig. 3F).

Analysis of immune cell infiltration (Supplementary Table S5) revealed that Cluster C2 is characterized by a relatively less active immune response, with high levels of naive B cells, resting memory T cells, and M0 macrophages (Fig. 3G). This suggests an immune environment where immune cells are either in a resting or naive state, possibly indicating immune tolerance or an inability to effectively respond to the tumor. Cluster C1, on the other hand, exhibits higher levels of memory B cells, CD8⁺ T cells, activated CD4⁺ T cells, follicular helper T cells,

regulatory T cells, NK cells, and monocytes, suggesting a more active immune response. However, the presence of regulatory T cells (Tregs) and monocytes indicates that the immune response might be suppressed or compromised, potentially favoring tumor survival (Fig. 3G). Together, these findings reveal that tumors in Cluster C1 may be undergoing a more active immune response, but with immune evasion mechanisms in place (e.g., Tregs), while tumors in Cluster C2 may be in a more immune-suppressive or immune-tolerant state, with a less effective immune response overall.

Moreover, the results highlight that distinct metabolic profiles are closely associated with immune activity and tumor purity, offering valuable insights into the interplay between metabolism and TIME in HNSCC.

3.3. Identification of metabolism-related gene clusters and their association with TIME in HNSCC

To further explore the functional implications of metabolism in HNSCC, differentially expressed genes (DEGs) between the initial metabolic clusters (C1 and C2) were identified using the R package "limma" (Supplementary Table S6). A total of 698 DEGs were classified as metabolism-related genes (Fig. 4A). Functional enrichment analysis of the MRGs identified pathways such as PI3K-Akt signaling, focal adhesion, and ECM-receptor interaction as significantly enriched, suggesting their potential roles in tumor progression and immune regulation 15-17 (Fig. 4B).

Prognostic analysis using univariate Cox regression was performed on these MRGs, identifying 142 representative prognosis-related MRGs (Supplementary Table S7). Based on the expression profiles of these 142 MRGs, HNSCC patients were classified into two distinct subgroups, designated as MRG-related clusters MC1 and MC2 (Fig. 4C) (Supplementary Table S8).

However, there was no significant difference in metabolic pathways between the MC1 and MC2 groups (Fig. 4D). Notably, Kaplan–Meier survival analysis demonstrated that MC2 had significantly longer OS compared to MC1 (p < 0.0001) (Fig. 4E).

Immune microenvironment analysis showed that Cluster MC2 is characterized by higher levels of naive B cells, plasma cells, and T cells (Fig. 4F), which suggests an immune environment with a mixed immune response, potentially with some activation of humoral and cellular immunity. However, the presence of naive immune cells may also imply a less effective or incomplete immune response, possibly due to immune tolerance or insufficient antigen presentation. Cluster MC1, on the other hand, shows higher levels of M0 and M2 macrophages, which suggests a more immune-suppressive tumor microenvironment. The high levels of M2 macrophages in particular indicate that the tumor may be using immune-suppressive mechanisms to promote growth and evade immune surveillance. From these results, it is clear that tumors in Cluster MC2 may be characterized by an ongoing but potentially ineffective immune response, while tumors in Cluster MC1 may have a more suppressive immune environment, favoring tumor progression and immune evasion.

Moreover, MC2 demonstrated significantly elevated expression of immune checkpoint molecules, including CTLA4, VSIR, and LAG3, which supports a more immune-active phenotype (Fig. 4G).

These analyses support the notion that the classification of HNSCC patients based on prognosis-related MRGs provides valuable insights into the metabolic and immune heterogeneity of the tumor microenvironment, with implications for prognosis and therapeutic strategies.

Interestingly, no significant metabolic differences were observed between the MC1 and MC2 groups. However, there were notable differences in the TIME and overall survival, suggesting that the mechanisms underlying metabolism-related genes and immune regulation are more complex than a simple linear relationship. While metabolic pathway alterations appeared limited, it is possible that the immune microenvironment is influenced by the cumulative effect of subtle metabolic changes, which may not be readily captured by bulk-level

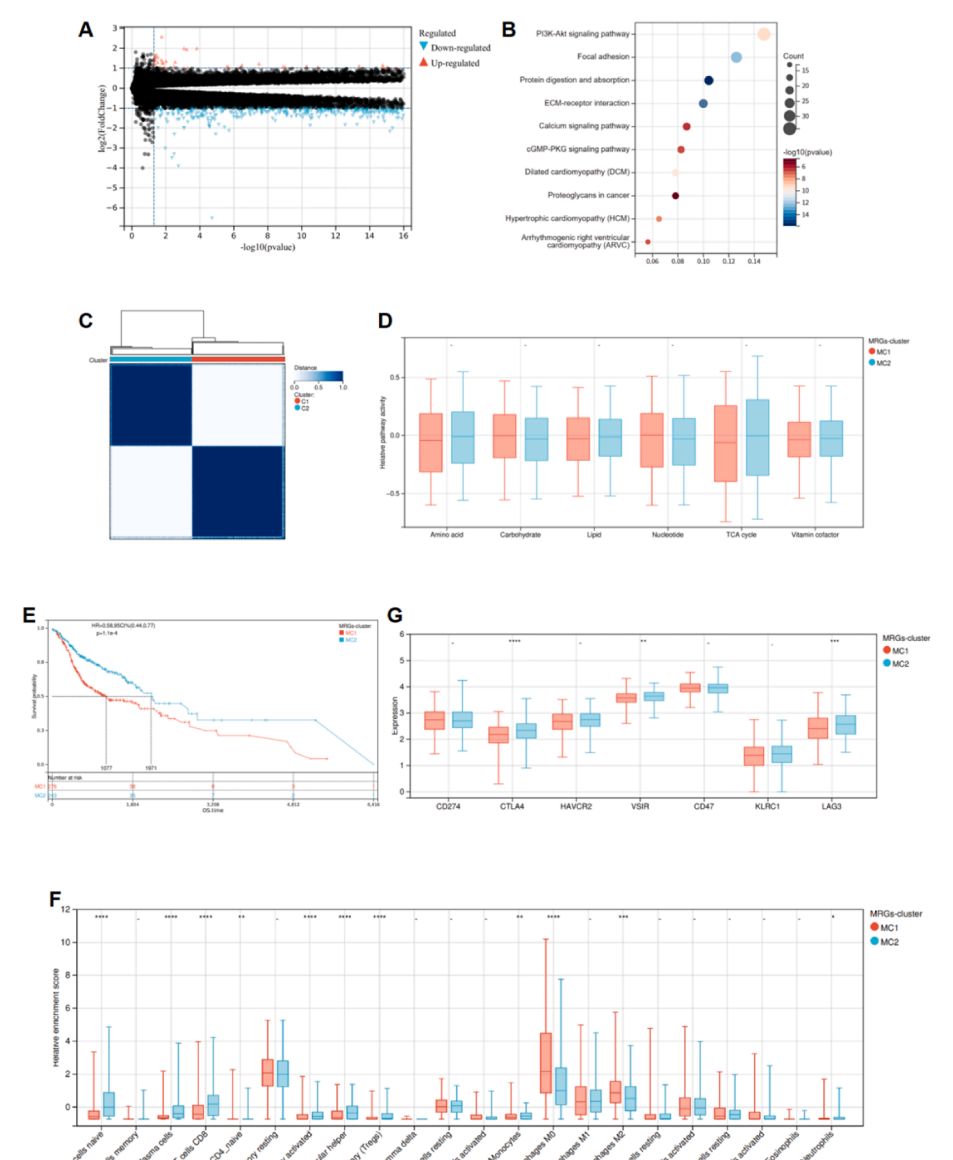


Fig. 4. Identification of metabolism-related gene clusters and their association with TIME in HNSCC. A. Volcano plot showing the differentially expressed genes (DEGs) between the metabolic clusters C1 and C2. B. Bubble plot showing enriched pathways from KEGG analysis of the MRGs. C. Heatmap of unsupervised clustering based on MRGs, dividing the samples into two MRG-related clusters (MC1 and MC2), D. Boxplots comparing the GSVA scores of the six key metabolic pathways between MC1 and MC2. E. Kaplan-Meier survival curve demonstrating OS differences between MC1 and MC2. F. Boxplots illustrating differences in immune cell infiltration scores between MC1 and MC2. G. Boxplots showing the expression of immune checkpoint molecules between MC1 and MC2. *P < 0.05. **P < 0.01. ***P < 0.001. ****P < 0.0001, compared to MC1.

pathway analysis. Furthermore, non-metabolic factors such as epigenetic modifications, stromal composition, or cytokine-mediated signaling may also contribute to shaping the immune landscape. These findings highlight the intricate and multifactorial nature of tumor immune regulation and underscore the need for integrated multi-omic approaches to fully elucidate these interactions.

3.4. Construction of a metabolism-related risk model and its association with the TIME

From the 142 prognosis-related MRGs identified in the previous section, LASSO regression analysis was performed to select 32 key prognosis-related MRGs (Supplementary Table S9). Next, stepwise multivariate Cox regression analysis was performed to develop an optimal risk model, which incorporated 16 core MRGs as the predictive signature. Risk scores for each sample were calculated based on the expression levels of these 16 genes (Supplementary Table S10). ROC curve analysis validated the reliability of the risk model, with an AUC

value above 0.7 for predicting 1-year, 3-year, and 5-year OS (Fig. 5A).

Patients were divided into high-risk and low-risk groups based on the optimal cutoff value of the calculated risk score. Survival analysis demonstrated that patients in the high-risk group had significantly worse OS compared to the low-risk group (P < 0.0001, HR = 0.35 [95% CI: 0.28–0.50]) (Fig. 5B).

Functional analysis revealed significant enrichment of the 16 core MRGs in pathways associated with tumor metabolism and immune regulation. Notably, patients in the high-risk group exhibited lower infiltration of immune cells, such as B cells and CD8⁺ T cells, compared to the low-risk group (Fig. 5C). This suggests a more immunosuppressive microenvironment in high-risk patients, which may contribute to their poorer prognosis.

The sankey plot (Fig. 5D) illustrates the progression from metabolic clusters (C1 and C2) to MRG-related clusters (MC1 and MC2). The majority of high-risk samples are derived from MC1, while most of the MC2 samples are classified into the low-risk group.

The results display two different visualizations of the key MRGs

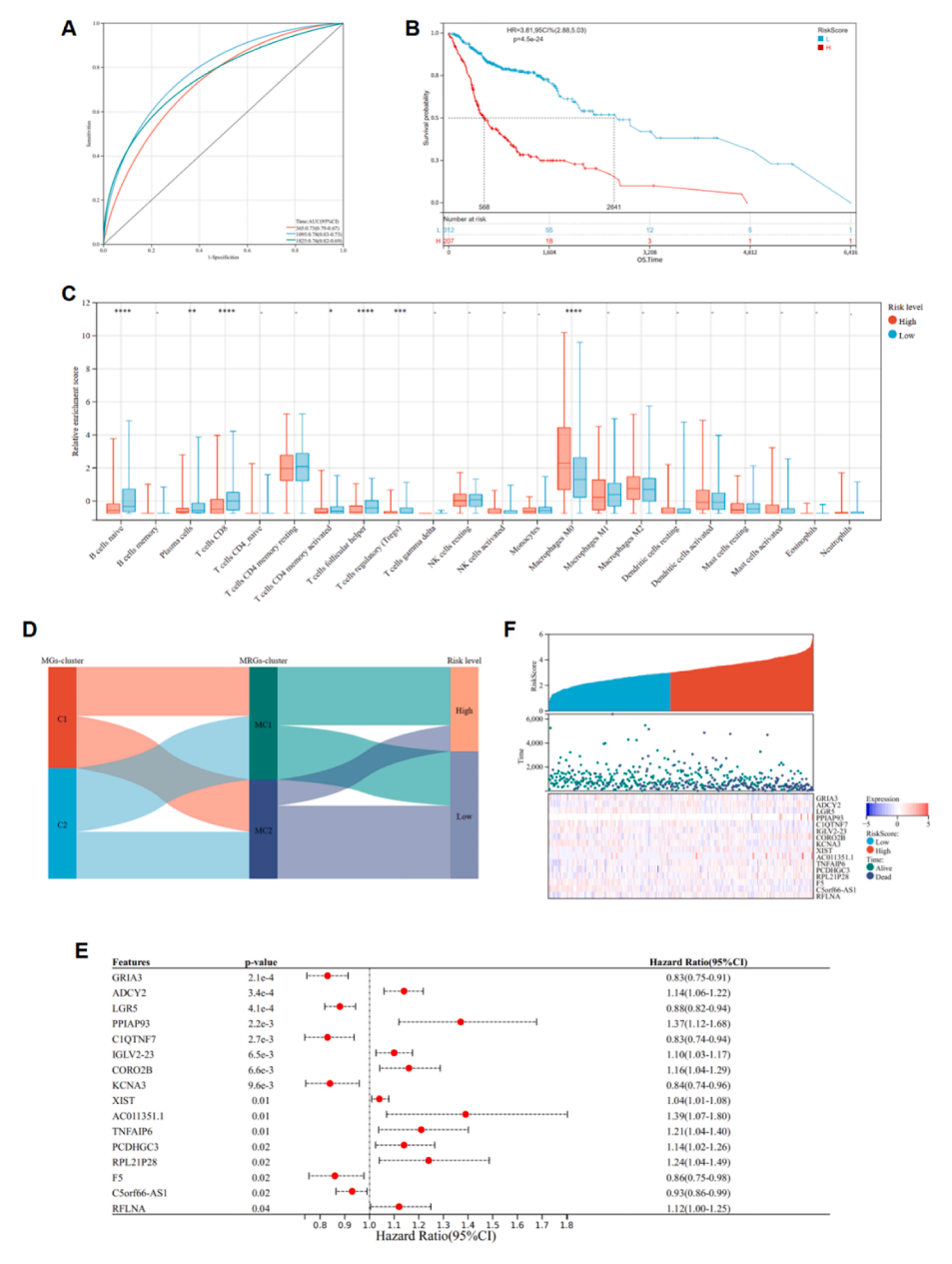


Fig. 5. Construction of a metabolism-related risk model and its association with the TIME. **A.** ROC curves for predicting 1-year, 3-year, and 5-year OS. **B.** KM survival curves comparing OS between high-risk and low-risk groups. **C.** Comparisons of immune cell infiltration levels between high-risk and low-risk groups. $^*P < 0.05$, $^{**P} < 0.01$, $^{***P} < 0.001$, $^{***P} < 0.001$, $^{***P} < 0.001$, compared to the low-risk group. **D.** Sankey diagram illustrating the cross-correlation between metabolism pathways, MRGs, and risk scores. **E.** Multivariate Cox regression analysis of the 16 core MRGs in the risk model. **F.** Heatmap showing the relationship between the expression levels of 16 core MRGs and survival prognosis.

identified in the multi-factorial Cox regression analysis and their association with survival prognosis. In Fig. 5E, a forest plot illustrates the hazard ratios (HRs) of the 16 core MRGs identified from the Cox regression model. The HR values for each gene are shown along with their corresponding 95% confidence intervals (CIs). This plot highlights that genes such as *ADCY2* and *TNFAIP6* are associated with an increased risk of poor survival prognosis (Fig. 5E).

The heatmap illustrates the expression levels of the identified MRGs across different samples. The heatmap highlights the differential expression of these genes in relation to survival prognosis, providing a visual representation of how gene expression correlates with survival outcomes. The survival prognosis-expressions are generally consistent with the HRs shown in the forest plot (Fig. 5F).

To further validate the prognostic value and immunological relevance of the metabolism-related risk model, we conducted an external validation using the GSE65858 dataset. Consistent with the training cohort, KM survival analysis showed that patients in the high-risk group

had significantly worse OS compared to those in the low-risk group (Fig. 6A, Supplementary Table S10). The time-dependent ROC curves demonstrated good predictive accuracy of the risk model for 1-, 3-, and 5-year survival, with AUCs of 0.69, 0.72, and 0.71, respectively (Fig. 6B). In addition, compared to the low-risk group, analysis of the tumor immune microenvironment revealed that patients in the high-risk group exhibited significantly higher stromal and immune scores, and lower tumor purity (Fig. 6C), further supporting the model's association with a distinct immune landscape.

In conclusion, this metabolism-related risk model provides a robust tool for predicting prognosis and reflects the immune microenvironment's heterogeneity in HNSCC patients, offering potential implications for personalized therapy.

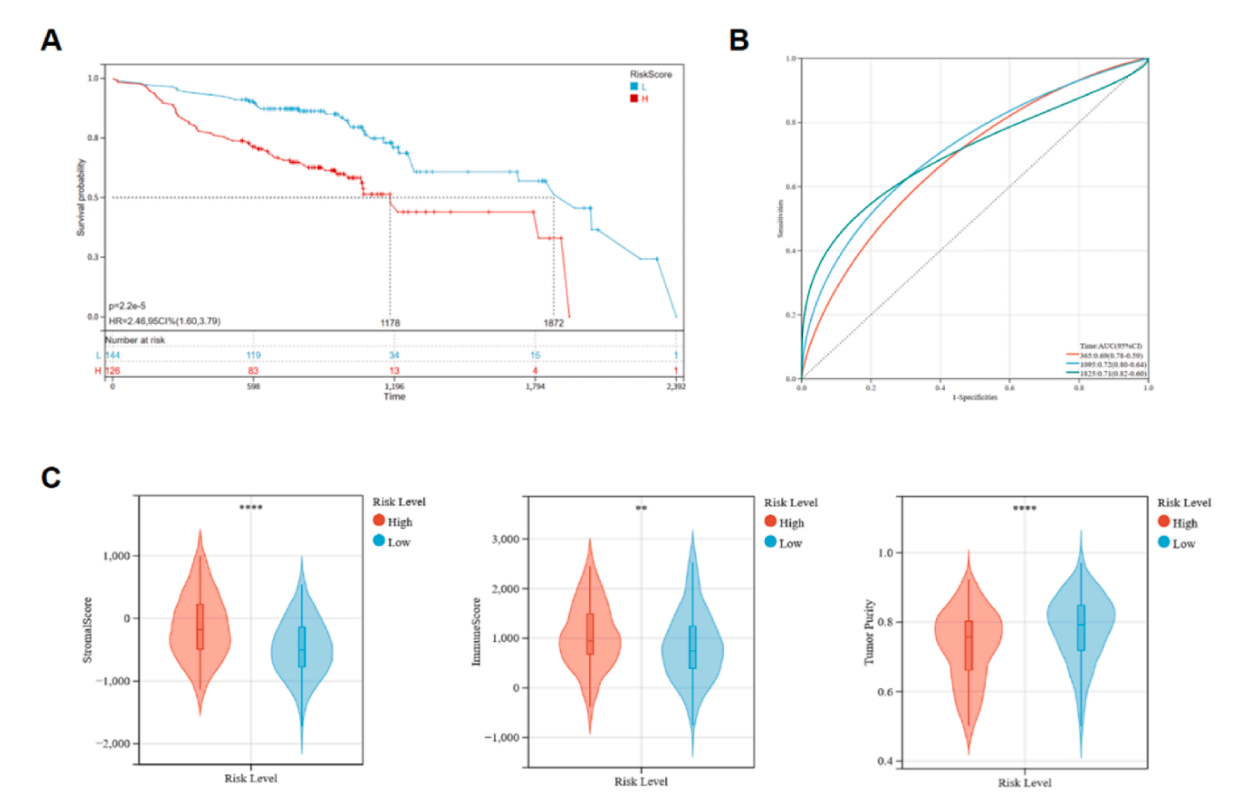


Fig. 6. External validation of the metabolism-related risk model in the GSE65858 cohort. **A.** KM survival analysis showing that patients in the high-risk group had significantly worse overall survival compared to those in the low-risk group. **B.** ROC curves of the risk model predicting 1-, 3-, and 5-year overall survival, with AUCs of 0.69, 0.72, and 0.71, respectively. **C.** Comparison of Stromalscore, Immunescore, and Tumor purity between high- and low-risk groups based on the ESTIMATE algorithm. *P < 0.05, **P < 0.01, ***P < 0.001, ***P < 0.001, ***P < 0.0001, **P < 0.0001, **P < 0.0001, **P < 0.0001, ***P < 0.0001, **P <

3.5. TNFAIP6 is overexpressed in cancer cells and strongly linked to TIME of HNSCC

In our study, we aimed to focus on genes positively associated with risk (HR >1) for further functional validation, as these genes are more likely to contribute to tumor progression and may serve as potential therapeutic targets. Although GRIA3 showed the most significant *P*-value (P=2.1e-4) and a relatively narrow confidence interval (HR =0.83), it exhibited a HR less than 1, indicating a potential protective role rather than a risk-associated effect (Fig. 5 E). Therefore, GRIA3 was not selected for further investigation.

Among the genes with HR>1, the top three—AC011351.1, PPIAP93, and PCDHGC3—either belong to pseudogenes or lack sufficient functional annotation and experimental validation in cancerrelated studies. These limitations make them less suitable for downstream mechanistic exploration.

We therefore selected *TNFAIP6*, which ranked fourth among the risk-associated genes (HR = 1.21, P = 0.01). *TNFAIP6* is a well-annotated protein-coding gene with documented roles in inflammation and cancer. Its biological relevance and availability of validated experimental tools made it a feasible and meaningful candidate for further functional studies in the context of tumor progression and immune regulation.

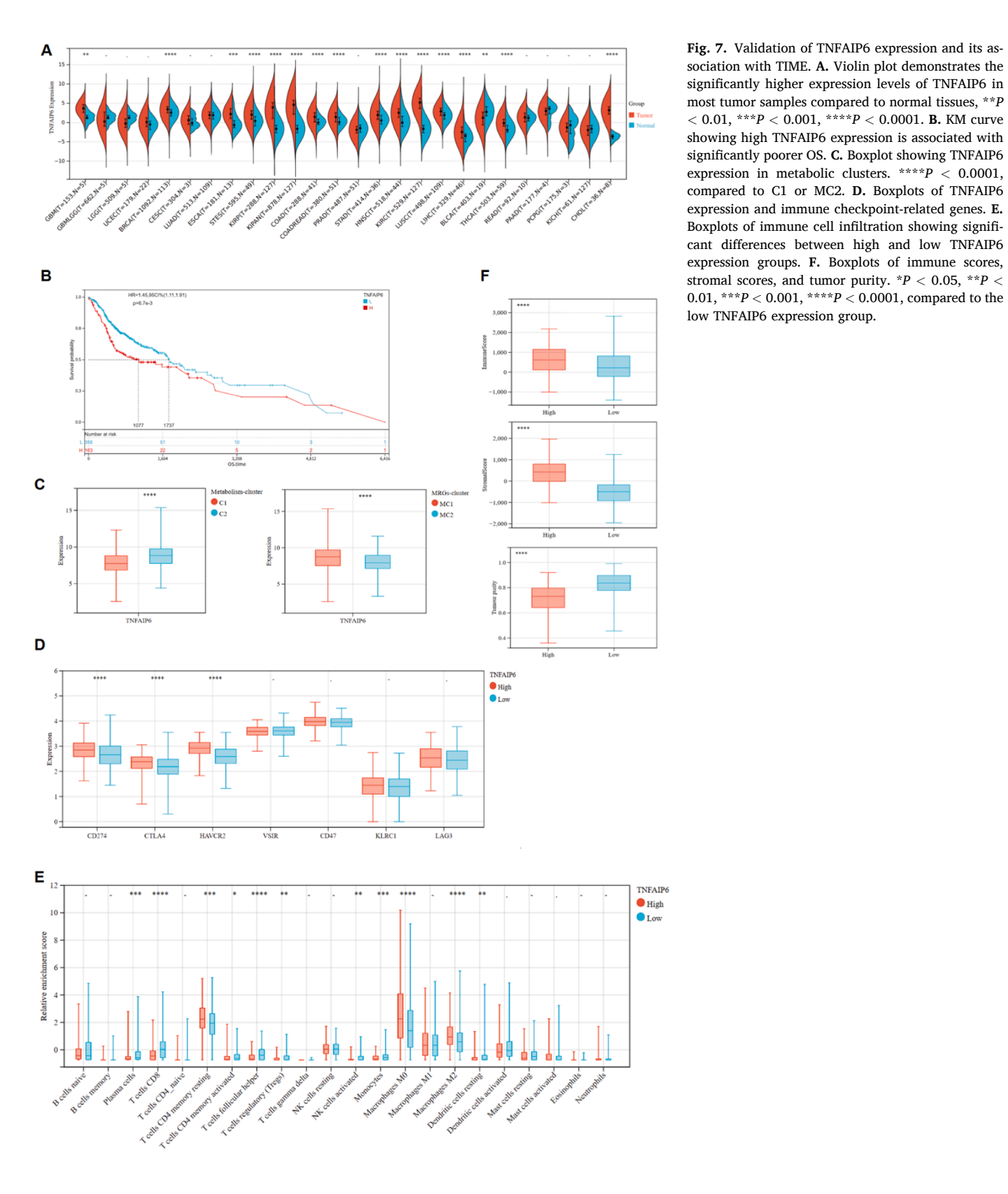
We first investigated TNFAIP6 expression across pan-cancer datasets and found that TNFAIP6 is significantly overexpressed in most tumor tissues compared to normal ones (Fig. 7A). TNFAIP6, also known as TNF- α -induced protein 6, is involved in various cellular processes, including inflammation and tissue remodeling. ¹⁸ Recent studies have highlighted its possible involvement in tumor growth and immune regulation. ¹⁹ Elevated TNFAIP6 expression has been linked to tumor development, immune escape, and poor prognosis in several cancer types, suggesting its importance in cancer biology and as a potential treatment target. ^{20,21}

To further validate the risk model, TNFAIP6 was selected for analysis as it showed a significant HR in the risk model, excluding pseudogenes. Using the optimal cutoff value for TNFAIP6 expression, patients were categorized into high- and low-expression groups. Kaplan-Meier survival analysis showed that high TNFAIP6 expression was linked to significantly poorer OS (Fig. 7B). TNFAIP6 expression was significantly higher in metabolic cluster C2 and MRG-related cluster MC1 compared to C1 and MC2, respectively (P < 0.0001), indicating its strong association with these high-risk patient subgroups (Fig. 7C).

TNFAIP6 expression showed positive correlations with several immune checkpoint-related genes, including *PD-L1*, *HAVCR2*, and *CTLA4* (Fig. 7D). Patients with high TNFAIP6 expression exhibited significantly higher levels of these checkpoint genes (P < 0.05). Infiltration analysis demonstrated notable differences between the high and low TNFAIP6 expression groups. High levels of TNFAIP6 are associated with lower infiltration of CD4⁺ and CD8⁺ T cells, and higher levels of M0 and M2 macrophages (Fig. 7E). This suggests that TNFAIP6 may be involved in immune evasion by inhibiting T cell activity and promoting M2 macrophage polarization. Combined with the data from Fig. 7D, which shows a positive correlation between TNFAIP6 and PD-L1 expression, we hypothesize that TNFAIP6 may influence T cell activity through the regulation of PD-L1 (P < 0.05).

Compared to the low-expression group, the high TNFAIP6 expression group had significantly higher immune scores, stromal scores, and tumor purity (P<0.0001), reflecting its association with immune microenvironment modulation.

To externally validate the association between TNFAIP6 expression, patient prognosis, and immune characteristics, we analyzed the GSE65858 dataset. Consistent with the TCGA results, KM survival analysis in the GSE65858 cohort revealed that patients with high TNFAIP6 expression had significantly worse OS (Fig. 8A). Moreover, high TNFAIP6 expression was associated with significantly elevated



stromal scores, immune scores, and decreased tumor purity (Fig. 8B), further highlighting its link to TIME. Immune infiltration analysis using the TIMER algorithm demonstrated that patients in the high-expression group exhibited increased infiltration of neutrophils, macrophages, and

dendritic cells (Fig. 8C).

These findings reinforce the role of TNFAIP6 and highlight its potential as a prognostic biomarker and immunomodulatory target in HNSCC.

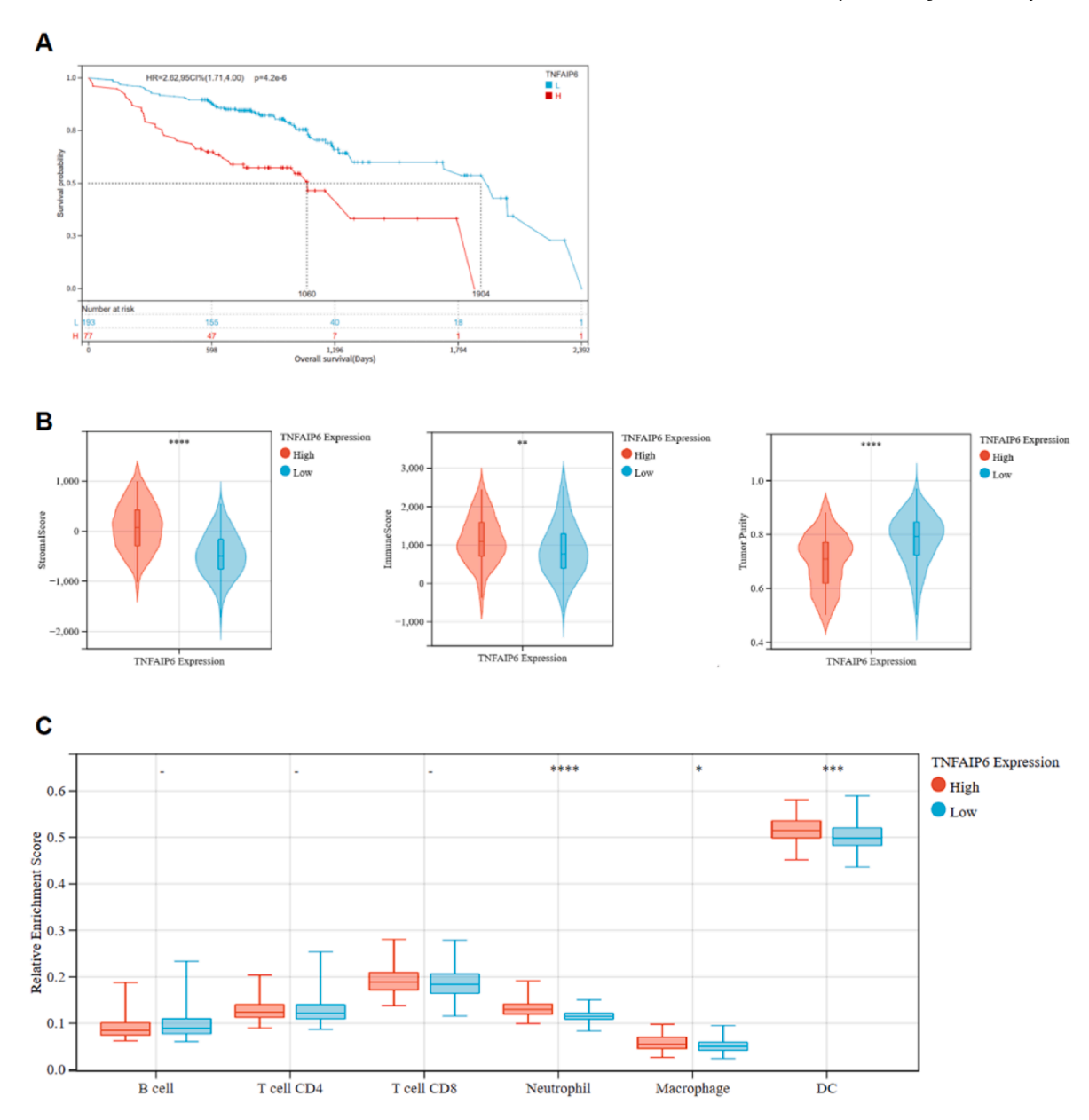


Fig. 8. External validation of the association between TNFAIP6 expression, survival, and immune characteristics in the GSE65858 cohort. **A.** Kaplan–Meier survival analysis showing that patients with high TNFAIP6 expression had significantly poorer overall survival. **B.** Comparison of stromal score, immune score, and tumor purity between high and low TNFAIP6 expression groups. **C.** Immune cell infiltration analysis based on the TIMER database. DC: dendritic cells. *P < 0.05, **P < 0.01, ***P < 0.001, ***P < 0.001, compared to the low TNFAIP6 expression group.

3.6. TNFAIP6 is a potential prognostic marker and associated with tumor progression

To further validate the role of TNFAIP6 in HNSCC, we performed a series of *in vitro* experiments following TNFAIP6 knockdown in HSC-6 and CAL-27. These experiments included cell proliferation, colony formation, migration, and invasion assays to assess the impact of TNFAIP6 depletion on tumor cell behavior.

Preliminary results indicate that knockdown of TNFAIP6 led to a significant reduction in cell proliferation, colony formation, migration, and invasion (Fig. 9A–E), consistent with our hypothesis that TNFAIP6 plays a role in promoting tumor growth and metastasis. These findings support the idea that TNFAIP6 may contribute to the aggressiveness of HNSCC and its potential as a therapeutic target.

This study preliminarily suggests that TNFAIP6 may play a role in promoting tumor cell migration in HNSCC. In recent years, increasing evidence has highlighted the involvement of TNFAIP6 in the

proliferation and metastasis of various cancers. For instance, TNFAIP6 is significantly upregulated in gastric cancer tissues and is associated with deeper tumor invasion, lymph node metastasis, and higher TNM stages. Knockdown of TNFAIP6 was shown to inhibit cell proliferation and migration, indicating its oncogenic potential. ²² In hepatocellular carcinoma, TNFAIP6 has been reported to promote tumor progression by enhancing glycolysis through the c-Myc/PKM2 axis. ²³ Furthermore, studies in urothelial carcinoma revealed that high TNFAIP6 expression is strongly correlated with poor prognosis and serves as an independent predictor of disease-specific and metastasis-free survival. ²⁴

Although the role of TNFAIP6 in promoting tumor development has been validated in several types of solid tumors, its molecular function and regulatory mechanisms in HNSCC remain largely unexplored. Future investigations may focus on whether TNFAIP6 exerts its effects through classical oncogenic pathways such as Wnt/ β -catenin or others.

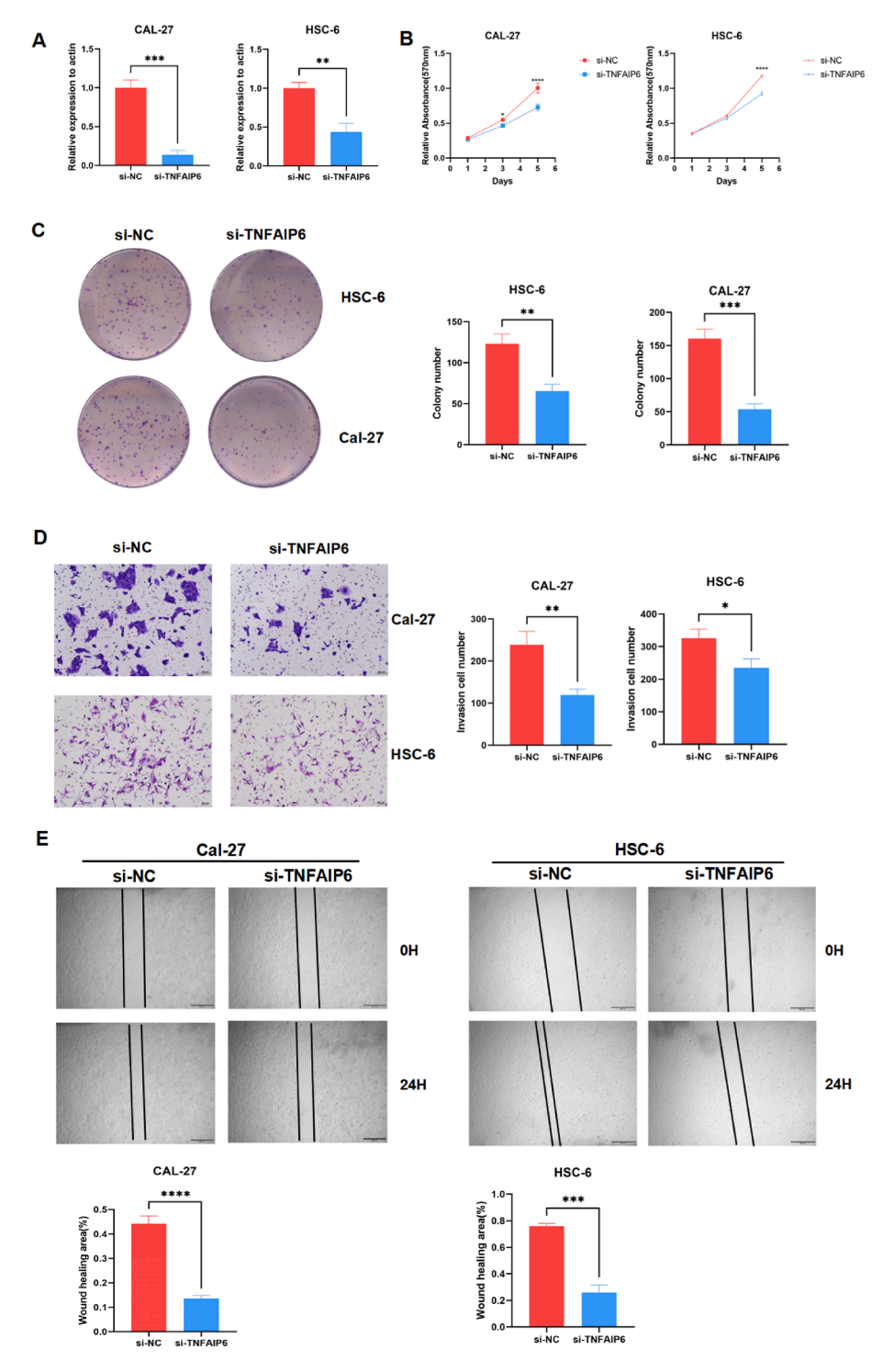


Fig. 9. Functional validation of TNFAIP6 knockdown in HNSCC cells. **A.** qPCR analysis showing the efficient knockdown of TNFAIP6 expression in HNSC cells. **B.** MTT assay demonstrating the effect of TNFAIP6 knockdown on HNSC cell proliferation. **C.** Colony formation assay showing the impact of TNFAIP6 knockdown on HNSC cell clonogenicity. **D.** Invasion assay showing the reduced invasive ability of TNFAIP6 knockdown HNSC cells. **E.** Scratch wound healing assay showing that TNFAIP6 knockdown suppressed the migration of HNSC cells. Si-NC: normal cell group; si-TNFAIP6: TNFAIP6 knockdown cell group. * $^{*}P < 0.05$, * $^{*}P < 0.01$, * $^{**}P < 0.001$, * $^{**}P < 0.001$, * $^{**}P < 0.001$, compared to the si-NC group.

4. Discussion

The integration of metabolic and immune profiles provides a more nuanced understanding of HNSCC biology and identifies TNFAIP6 as a promising target for immunotherapy. Its role in immune checkpoint regulation makes it a potential candidate for combination therapy with checkpoint inhibitors, offering a new avenue for improving therapeutic outcomes in HNSCC patients. Furthermore, the risk model derived from this study could be used to stratify patients for personalized treatment

strategies, enhancing the precision of therapeutic interventions.

Several studies have reported that the expression level of TNFAIP6 is associated with the prognosis of HNSCC patients. 25 However, there is limited research on the relationship between TNFAIP6 and the immune microenvironment or tumor metabolism in HNSCC. 26 Our study expands on these findings by providing new insights into this relationship, suggesting that TNFAIP6 may not only affect tumor progression through its direct role in immune modulation but also influence tumor metabolism, thereby contributing to a more aggressive tumor phenotype. This dual

role opens up opportunities for targeting *TNFAIP6* in a more holistic therapeutic approach that addresses both immune evasion and metabolic reprogramming in tumors.

Our findings are in line with previous research on the immune-modulating effects of TNFAIP6, which has been implicated in various cancers. For instance, similar to our observations in HNSCC, TNFAIP6 has been shown to regulate immune checkpoints, such as PD-1/PD-L1, in other malignancies, including breast cancer and melanoma, ^{27,28} including head and neck cancer. ^{29,30} This supports the hypothesis that *TNFAIP6* could serve as a universal immune-modulating target across different tumor types, further establishing its importance in cancer immunotherapy. However, our study differs from earlier studies by revealing the specific role of TNFAIP6 in modulating the immune microenvironment in HNSCC, with a particular focus on macrophage polarization and T cell exclusion, which has not been as extensively explored in other cancers.

Although the precise mechanisms by which TNFAIP6 contributes to immune regulation remain to be fully elucidated, our data suggest that TNFAIP6 may facilitate tumor immune evasion through multiple pathways. The positive correlation between TNFAIP6 expression and key immune checkpoint molecules such as PD-L1, CTLA4, and HAVCR2 implies that TNFAIP6 may be involved in the upregulation of inhibitory immune signals, thereby dampening T cell-mediated anti-tumor immunity. In addition, tumors with high TNFAIP6 expression were characterized by reduced CD4⁺ and CD8⁺ T cell infiltration and increased M0 and M2 macrophage presence, indicating a shift toward an immunosuppressive microenvironment. Given the known role of M2 macrophages in promoting tumor progression and suppressing adaptive immune responses, it is plausible that TNFAIP6 promotes macrophage polarization and T cell exclusion. Previous studies have demonstrated that TNFAIP6 interacts with hyaluronan and contributes to extracellular matrix remodeling, 31,32 which may influence immune cell trafficking and activation. Taken together, these findings support the hypothesis that TNFAIP6 may act as an immunoregulatory molecule in the tumor microenvironment, potentially through modulating PD-L1 expression and macrophage phenotype, warranting further mechanistic investigation.

While this study provides some insights, there are some limitations. First, the findings are based on bioinformatics and preliminary *in vitro* experiments, necessitating further validation in preclinical and clinical settings. Second, the underlying mechanisms of TNFAIP6 in regulating immune checkpoints and its interaction with metabolic pathways warrant deeper investigation. Future studies should focus on elucidating these mechanisms and evaluating the synergistic effects of targeting TNFAIP6 with existing immunotherapies in HNSCC. Additionally, exploring the potential of combining TNFAIP6 inhibition with metabolic modulators could provide new therapeutic strategies that simultaneously disrupt tumor metabolism and enhance immune responses.

Finally, clinical trials are necessary to assess the potential of targeting TNFAIP6 alongside other treatments, like immune checkpoint inhibitors or metabolic drugs. Long-term studies on the link between TNFAIP6 expression and how patients respond to immunotherapy could offer useful information on its role as a biomarker and treatment target.

5. Conclusion

In conclusion, our study highlights the important role of metabolic pathways in influencing the immune environment of HNSCC and identifies TNFAIP6 as a key factor. By connecting metabolic reprogramming and immune regulation, TNFAIP6 serves as a novel prognostic marker and a potential target for immunotherapy, paving the way for more effective and personalized treatment strategies in HNSCC.

CRediT authorship contribution statement

Meina Lian: Writing – original draft, Data curation. Xiaoxia Wang:

Data curation. **Zixian Huang:** Data curation. **Yudong Wang:** Writing – review & editing, Conceptualization. **Zhiquan Huang:** Writing – review & editing, Conceptualization.

Funding

This work was supported by grants from the National Natural Science Foundation of China (No. 82303563), the Science and Technology Program of Guangdong (No. 2023A1515010567), the Guangzhou Science and Technology Project (No. 2023B03J1242).

Declaration of competing interest

The authors declare that they have no known competing financial interests or personal relationships that could have appeared to influence the work reported in this paper.

Abbreviations

HNSCC Head and Neck Squamous Cell Carcinoma

TIME Tumor immune microenvironment

MRGs Metabolism-related genes
TCA Tricarboxylic acid

GSVA Gene set variation analysis

OS Overall survival

KM Kaplan-Meier

CDF Cumulative distribution function
DEGs Differentially expressed genes

KEGG Kyoto encyclopedia of genes and genomes

ICB Immune checkpoint blockade

TNFAIP6 Tumor necrosis factor α-inducible protein 6

ROC Receiver operating characteristic

AUC Area under the time-dependent ROC curve LASSO Least absolute shrinkage and selection operator

HAVCR2 Hepatitis A virus cellular receptor 2

CTLA4 Cytotoxic T-lymphocyte associated protein 4

LAG3 Lymphocyte activating 3 VSIR V-set immunoregulatory receptor KLRC1 killer cell lectin like receptor C1

Appendix A. Supplementary data

Supplementary data to this article can be found online at https://doi.org/10.1016/j.jhip.2025.06.006.

References

- Barsouk A, Aluru JS, Rawla P, et al. Epidemiology, risk factors, and prevention of head and neck squamous cell carcinoma. Med Sci. 2023;11(2):42.
- Yilmaz E, Ismaila N, Bauman JE, et al. Immunotherapy and biomarker testing in recurrent and metastatic head and neck cancers: ASCO guideline. J Clin Oncol. 2023; 41(5):1132–1146.
- Hanahan D, Weinberg RA. Hallmarks of cancer: the next generation. Cell. 2011;144 (5):646–674.
- Faubert B, Solmonson A, DeBerardinis RJ. Metabolic reprogramming and cancer progression. Science. 2020;368(6487):5473.
- Smyth MJ, Ngiow SF, Ribas A, et al. Combination cancer immunotherapies tailored to the tumour microenvironment. Nat Rev Clin Oncol. 2016;13(3):143–158.
- Kao KC, Vilbois S, Tsai CH, et al. Metabolic communication in the tumour-immune microenvironment. Nat Cell Biol. 2022;24(11):1574–1583.
- Liu S, Wang S, Wang Z. Identification of genetic mechanisms underlying lipid metabolism-mediated tumor immunity in head and neck squamous cell carcinoma. BMC Med Genom. 2023;16(1):110.
- Huang PC, Chang CW, Lin YC, et al. Pyruvate kinase differentially alters metabolic signatures during head and neck carcinogenesis. Int J Mol Sci. 2023;24(23):16639.
- Peng X, Chen Z, Farshidfar F, et al. Molecular characterization and clinical relevance of metabolic expression subtypes in human cancers. *Cell Rep.* 2018;23(1):255–269. e4.
- Wilkerson MD, Hayes DN. ConsensusClusterPlus: a class discovery tool with confidence assessments and item tracking. Bioinformatics. 2010;26(12):1572–1573.

- Yoshihara K, Shahmoradgoli M, Martínez E, et al. Inferring tumour purity and stromal and immune cell admixture from expression data. Nat Commun. 2013;4: 2612
- Gong S, Wu C, Köhler F, et al. Procollagen-lysine, 2-oxoglutarate 5-dioxygenase family: novel prognostic biomarkers and tumor microenvironment regulators for lower-grade glioma. Front Cell Neurosci. 2022;16:838548.
- Newman AM, Liu CL, Green MR, et al. Robust enumeration of cell subsets from tissue expression profiles. Nat Methods. 2015;12(5):453–457.
- Blanche P, Dartigues JF, Jacqmin GH. Estimating and comparing time-dependent areas under receiver operating characteristic curves for censored event times with competing risks. Stat Med. 2013;32(30):5381–5397.
- Brugge J, Hung MC, Mills GB. A new mutational AKTivation in the PI3K pathway. Cancer Cell. 2007;12(2):104–107.
- Yuan Z, Li Y, Zhang S, et al. Extracellular matrix remodeling in tumor progression and immune escape: from mechanisms to treatments. Mol Cancer. 2023;22(1):48.
- Jiang H, Hegde S, Knolhoff BL, et al. Targeting focal adhesion kinase renders pancreatic cancers responsive to checkpoint immunotherapy. *Nat Med.* 2016;22(8): 851–860
- Day AJ, Milner CM. TSG-6: a multifunctional protein with anti-inflammatory and tissue-protective properties. *Matrix Biol*. 2019;78–79:60–83.
- Chan TC, Li CF, Ke HL, et al. High TNFAIP6 level is associated with poor prognosis of urothelial carcinomas. *Urol Oncol*. 2019;37(4):293 e11–293 e24.
- 20. Gu G, Lv X, Liu G, et al. Tnfaip6 secreted by bone marrow-derived mesenchymal stem cells attenuates TNBS-induced colitis by modulating follicular helper T cells and follicular regulatory T cells balance in mice. Front Pharmacol. 2021;12:734040.
- Li L, Yang L, Chen X, et al. TNFAIP6 defines the MSC subpopulation with enhanced immune suppression activities. Stem Cell Res Ther. 2022;13(1):479.

- Zhang X, Xue J, Yang H, et al. TNFAIP6 promotes invasion and metastasis of gastric cancer and indicates poor prognosis of patients. Tissue Cell. 2021;68:101455.
- Duan K, Fang K, Sui C. TFAIP6 facilitates hepatocellular carcinoma cell glycolysis through upregulating c-myc/PKM2 axis. Heliyon. 2024;10(10):e30959.
- Chan TC, Li CF, Ke HL, et al. High TNFAIP6 level is associated with poor prognosis of urothelial carcinomas. *Urol Oncol: Seminars and Original Investigations*. 2019;37(4): 293.e11–293.e24.
- Lan G, Yu X, Sun X, et al. Comprehensive analysis of the expression and prognosis for TNFAIPs in head and neck cancer. Sci Rep. 2021;11(1):15696.
- 26. Wang J, Lin F, Zhou Y, et al. Chemopreventive effect of modified zeng-sheng-ping on oral squamous cell carcinoma by regulating tumor associated macrophages through targeting tnf alpha induced protein 6. BMC Complement Med Ther. 2024;24(1):287.
- Keir ME, Butte MJ, Freeman GJ, et al. PD-1 and its ligands in tolerance and immunity. Annu Rev Immunol. 2008;26:677–704.
- Sun C, Mezzadra R, Schumacher TN. Regulation and function of the PD-L1 checkpoint. *Immunity*. 2018;48(3):434–452.
- 29. Burtness B, Harrington KJ, Greil R, et al. Pembrolizumab alone or with chemotherapy versus cetuximab with chemotherapy for recurrent or metastatic squamous cell carcinoma of the head and neck (KEYNOTE-048): a randomised, open-label, phase 3 study. *Lancet*. 2019;394(10212):1915–1928.
- Franken A, Bila M, Mechels A, et al. CD4(+) T cell activation distinguishes response to anti-PD-L1+anti-CTLA4 therapy from anti-PD-L1 monotherapy. *Immunity*. 2024; 57(3):541–558 e7.
- Milner CM, Day AJ. TSG-6: a multifunctional protein associated with inflammation. J Cell Sci. 2003;116(10):1863–1873.
- Lewis A, Steadman R, Manley P, et al. Diabetic nephropathy, inflammation, hyaluronan and interstitial fibrosis. *Histol Histopathol*. 2008;23(6):731–739.